Numerical Improvement of the Discrete Element Method applied to Shear of Granular Media

Andrés A. Peña[1], Pedro G. Lind[1,2], Sean McNamara[1], and Hans J. Herrmann[3,4]

[1] Institute for Computational Physics, Universität Stuttgart, Pfaffenwaldring 27, D-70569 Stuttgart, Germany
[2] Centro de Física Teórica e Computacional, Av. Prof. Gama Pinto 2, 1649-003 Lisbon, Portugal
[3] Departamento de Física, Universidade Federal do Ceará, 60451-970 Fortaleza, Ceará, Brazil
[4] Computational Physics, IfB, HIF E12, ETH Hönggerberg, CH-8093 Zürich, Switzerland

We present a detailed analysis of the bounds on the integration step in Discrete Element Method (DEM) for simulating collisions and shearing of granular assemblies. We show that, in the numerical scheme, the upper limit for the integration step, usually taken from the average time t_c of one contact, is in fact not sufficiently small to guarantee numerical convergence of the system during relaxation. In particular, we study in detail how the kinetic energy decays during the relaxation stage and compute the correct upper limits for the integration step, which are significantly smaller than the ones commonly used. In addition, we introduce an alternative approach, based on simple relations to compute the frictional forces, that converges even for integration steps above the upper limit.

1 Introduction

One of the standard approaches to model the dynamics of granular media is to use the Discrete Element Method (DEM) [1, 2, 3], e.g. to study shear [4, 5, 6, 7, 8]. Some problems may arise due to the need to use large integration steps to perform numerical simulations with reasonable computational effort, without compromising the overall convergence of the numerical scheme. For slow shearing, the convergence of the numerical schemes is particularly important when studying for instance the occurrence of avalanches [8] and the emergence of ratcheting in cyclic loading [9]. Usually, one assumes an upper limit for the admissible integration steps, based on empirical reasoning[10].

The aim of this paper is twofold. First, we show that an integration step able to guarantee convergence of the numerical scheme, must in general be smaller than a specific upper limit, significantly below the commonly accepted value [5, 10, 11]. This upper limit strongly depends on (i) the accuracy of the approach used to calculate frictional forces between particles, (ii) on the corresponding duration of the contact and (iii) on the number of degrees of freedom. Second, we address the specific case of slow shearing, for which the above limit is too small to allow for reasonable computation time. To overcome this shortcoming we propose an alternative

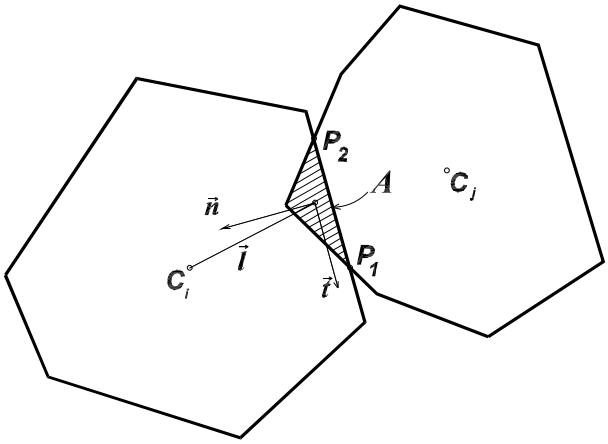

Fig. 1. Illustration of two overlapping particles. The overlap region A between particles fully characterizes the contact force $\boldsymbol{F}^c$ (see text).

approach that corrects the frictional contact forces, when large integration steps are taken. In this way, we enable the use of considerably larger integration steps, assuring at the same time the convergence of the integration scheme.

We start in Sec. 2 by presenting in some detail the Discrete Element Method [1, 10, 12]. Sections 3 and 4 describe respectively the dependence on the integration step and the improved algorithm. Discussions and conclusions are given in Sec. 5.

2 The model

We consider a two-dimensional system of polygonal particles, each one having two linear and one rotational degree of freedom. The evolution of the system is given by Newton's equations of motion, where the resulting forces and moments acting on each particle i are given by the sum of all forces and momenta applied on that particle:

$$m_i \ddot{\boldsymbol{r}}_i = \sum_c \boldsymbol{F}_i^c + \sum_{c_b} \boldsymbol{F}_i^b, \tag{1a}$$

$$I_i \ddot{\boldsymbol{\theta}}_i = \sum_c \boldsymbol{l}_i^c \times \boldsymbol{F}_i^c + \sum_{c_b} \boldsymbol{l}_i^b \times \boldsymbol{F}_i^b, \tag{1b}$$

where m_i denotes the mass of particle i, I_i its moment of inertia, and $\boldsymbol{l}$ the branch vector which connects the center of mass of the particle to the application point of the contact force $\boldsymbol{F}_i^c$ or boundary force $\boldsymbol{F}_i^b$. The sum in c is over all the particles in contact with polygon i, and the sum in c_b is over all the vertices of polygon i in contact with the boundary. One integrates Eqs. (1) for all particles $i = 1, \ldots, N$ and obtains the evolution of their centers of mass $\boldsymbol{r}_i$ and rotation angles θ_i.

Further, during loading, particles tend to deform each other. This deformation of the particles is usually reproduced by letting them overlap [1, 12], as illustrated in Fig. 1. The overlap between each pair of particles is considered to fully characterize the contact. Namely, the normal contact force is assumed to be proportional to the overlap area [17] and its direction perpendicular to the plane of contact, which is defined by the intersection between the boundaries of the two particles.

All the dynamics is deduced from the contact forces acting on the particles. The contact forces, $\boldsymbol{F}^c$, either between particles or with the boundary, are decomposed into their elastic and viscous contributions, $\boldsymbol{F}^e$ and $\boldsymbol{F}^v$ respectively, yielding $\boldsymbol{F}^c = \boldsymbol{F}^e + \boldsymbol{F}^v$.

The viscous force is important for maintaining the numerical stability of the method and to take into account dissipation at the contact. This force is calculated as [12]

$$\boldsymbol{F}^v = -m_r \nu \boldsymbol{v}^c, \tag{2}$$

where $m_r = (1/m_i + 1/m_j)^{-1}$ is the reduced mass of the two particles, i and j, and ν is the damping coefficient.

The elastic part of the contact force is what will be carefully studied, since it is what determines the accuracy of the integration scheme. The term $\boldsymbol{F}^e$ is simply given by the sum of the normal and the tangential components, with respect to the contact plane, namely

$$\boldsymbol{F}^e = F_n^e \hat{n}^c + F_t^e \hat{t}^c, \tag{3}$$

where the normal component reads

$$F_n^e = -k_n A / l_c, \tag{4}$$

with k_n the normal stiffness, A the overlap area and $l_c = r_i + r_j$ the characteristic length of the contact between particles i and j, with $r_i = \sqrt{A_i/2\pi}$ and A_i the area of the particle i (and similarly for particle j).

Using an extension of the Cundall-Stack spring [12], which considers the tangential force to be proportional to the elastic elongation ξ of an imaginary spring at the contact, one defines the static frictional force between each pair of particles in contact, as

$$F_t^e = -k_t \xi, \tag{5}$$

where k_t is the tangential stiffness. This tangential force assumes each contact as being described by a damped oscillator with some frequency ω (see below).

The elastic elongation ξ in Eq. (5) is updated as

$$\xi(t + \Delta t) = \xi(t) + \boldsymbol{v}_t^c \Delta t \tag{6}$$

where Δt is the time step of the DEM simulation, and $\boldsymbol{v}_t^c$ is the tangential component of the relative velocity

$$\boldsymbol{v}^c = \boldsymbol{v}_i - \boldsymbol{v}_j + \boldsymbol{w}_i \times \boldsymbol{l}_i - \boldsymbol{w}_j \times \boldsymbol{l}_j, \tag{7}$$

at the contact point. Here, $\boldsymbol{v}_i$ and $\boldsymbol{v}_j$ are the linear velocities of the centers of mass and $\boldsymbol{w}_i$ and $\boldsymbol{w}_j$ the angular velocities of the particles around the corresponding centers of mass.

The tangential elastic elongation ξ changes according to Eq. (6) whenever the condition $|F_e^t| < \mu F_e^n$ is satisfied, whereas, when the Coulomb limit condition $|F_e^t| = \mu F_e^n$ is reached, sliding is enforced by keeping constant the tangential force F_e^t and assigning to ξ its extreme values $\pm\mu k_n A/(k_t l_c)$. This latter Coulomb condition corresponds to the regime where particles behave inelastically, while the former inequality describes the forces when the particles behave elastically. Parameter μ is the inter-particle friction coefficient.

In DEM, one of the numerical integration schemes usually used to solve the equations of motion above is Gear's predictor-corrector scheme [10]. This scheme consist of three main stages, namely prediction, evaluation and correction.

In the prediction stage the linear and angular positions, velocities and higher-order time derivatives are updated by expansions in Taylor series using the current values of these quantities [10, 13]. In particular, one extracts a predicted position $\boldsymbol{r}^p(t+\Delta t)$ and acceleration $\ddot{\boldsymbol{r}}^p(t+\Delta t)$ for the center of mass of a given particle and the predicted angular displacement $\boldsymbol{\theta}^p(t+\Delta t)$ and angular acceleration $\ddot{\boldsymbol{\theta}}^p(t+\Delta t)$ of that particle around its center of mass.

During the evaluation stage, one uses the predicted coordinates to determine the contact force $\boldsymbol{F}^c_{t+\Delta t}$ at time $t+\Delta t$. Since the method is not exact, there is a difference between the acceleration $\ddot{\boldsymbol{r}}(t+\Delta t) = \boldsymbol{F}^c_{t+\Delta t}/m$ and the value obtained in the prediction stage, namely

$$\Delta\ddot{\boldsymbol{r}} = \ddot{\boldsymbol{r}}(t+\Delta t) - \ddot{\boldsymbol{r}}^p(t+\Delta t). \tag{8}$$

The difference $\Delta\ddot{\boldsymbol{r}}$ in Eq. (8) is then finally used in the corrector step to correct the predicted position and its time derivatives, using proper weights for each time derivative [10], that depend upon the order of the algorithm and the differential equation being solved. These corrected values are the ones used for the next integration step $t+\Delta t$. This same procedure is also applied to the rotation angles θ_i around the center of mass as well as to their time derivatives, yielding the correction $\Delta\ddot{\boldsymbol{\theta}}$.

In our simulations we integrate equations of the form $\ddot{\boldsymbol{r}} = f(\boldsymbol{r}, \dot{\boldsymbol{r}})$, using a fifth order predictor-corrector algorithm that has a numerical error proportional to $(\Delta t)^6$ for each integration step [10]. However, as will be seen in Sec. 3, $(\Delta t)^6$ is not the numerical error of the full integration scheme, since Eq. (5), used to calculate the frictional force, is of order $(\Delta t)^2$.

For a certain value of normal contact stiffness k_n, almost any value for the normal damping coefficient ν_n might be selected. Their relation defines the restitution coefficient ϵ obtained experimentally for various materials [14]. The restitution coefficient is given by the ratio between the relative velocities after and before a collision. In particular, the normal restitution coefficient ϵ_n can be written as a function of k_n and ν_n [15], namely

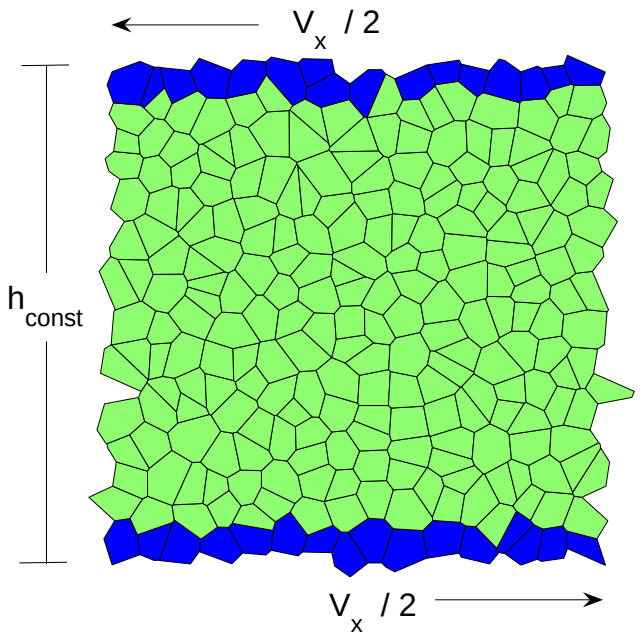

Fig. 2. (Color online) Sketch of the system of 256 particles (green particles) under shearing of top and bottom boundaries (blue particles). Horizontally periodic boundary conditions are considered and a constant low shear rate is chosen (see text).

$$\epsilon_n = \exp\left(-\pi\eta/\omega\right) = \exp\left(-\frac{\pi}{\sqrt{4m_r k_n/\nu_n^2 - 1}}\right) \tag{9}$$

where $\omega = \sqrt{\omega_0^2 - \eta^2}$ is the frequency of the damped oscillator, with $\omega_0 = \sqrt{k_n/m_r}$ the frequency of the elastic oscillator, m_r the reduced mass and $\eta = \nu_n/(2m_r)$ the effective viscosity. The tangential component ϵ_t of the restitution coefficient is defined similarly using k_t and ν_t in Eq. (9).

Therefore, a suitable closed set of parameters for this model are the ratios k_t/k_n and ϵ_t/ϵ_n (or ν_t/ν_n), together with the normal stiffness k_n and the interparticle friction μ.

The entire algorithm above relies on a proper choice of the integration step Δt, which should neither be too large to avoid divergence of the integration nor too small avoiding unreasonably long computational time. The determination of the optimal integration step varies from case to case and there are two main criteria to estimate an upper bound for admissible integration steps.

The first criterion is to use the characteristic period of oscillation [10], defined as

$$t_s = 2\pi\sqrt{\frac{\langle m\rangle}{k_n}}, \tag{10}$$

where $\langle m\rangle$ is the smallest particle mass in the system. For a fifth order predictor-corrector integration scheme, it is usually accepted that a safe integration step should be below a threshold of $\Delta t < t_s/10$ [10].

The second criterion is to extract the threshold from local contact events [5, 11, 15], namely from the characteristic duration of a contact:

$$t_c = \frac{\pi}{\sqrt{\omega_0^2 - \eta^2}}. \tag{11}$$

Typically $t_c \simeq t_s/2$, and therefore in such cases, one considers an admissible integration step as $\Delta t < t_c/5$ [15, 16].

In the next section we will study in detail the integration for different values of the model parameters.

3 The choice of the integration step

We simulate the relative motion of two plates shearing against each other [7, 8, 17]. Considering a system of 256 particles as illustrated in Fig. 2, where both top and bottom boundaries move in opposite directions with a constant shear rate $\dot\gamma$. The top and bottom layer of the sample have fixed boundary conditions, while horizontally we consider periodic boundary conditions. The volumetric strain is suppressed, i.e. the vertical position of the walls is fixed and there is no dilation. The particles of the fixed boundary are not allowed to rotate or move against each other. The shear rate is $\dot\gamma = 1.25 \cdot 10^{-5}\text{s}^{-1}$, the parameter values are $k_n = 400$ N/m, $\epsilon_n = 0.9875$, and $\mu = 0.5$. The relation k_t/k_n is chosen such that $k_t < k_n$, similarly to previous studies [12, 15, 18], namely $k_t/k_n = 1/3$. Further, for simplicity we consider $\nu_t/\nu_n = k_t/k_n$, which when substituted in Eq. (9) yields $\epsilon_t/\epsilon_n = 1.0053$.

By integrating such a system of particles using the scheme described in the previous section, one can easily compute the kinetic energy E_k of a given particle i,

$$E_k(i) = \frac{1}{2}\left(m_i\dot{\boldsymbol{r}}_i^2 + I_i\boldsymbol{\omega}_i^2\right), \tag{12}$$

where velocity $\dot{\boldsymbol{r}}$ is computed from the predictor-corrector algorithm, I_i is the moment of inertia of the polygon and $\boldsymbol{\omega}_i$ is the angular velocity.

In Fig. 3 we show the evolution of the kinetic energy for two different $\Delta t = 0.001$ s and 0.005 s. As one sees, frictionless particles (Fig. 3a and 3c) have an E_k that does not change for different integration steps, while when $\mu = 0.5$ (Fig. 3b and 3d) the evolution of E_k strongly depends on Δt. In Fig. 3e we plot the cumulative difference ΔE_k between the values of E_k taken for each integration step. Here, one sees that in the absence of friction ΔE_k is significantly lower then when friction is present.

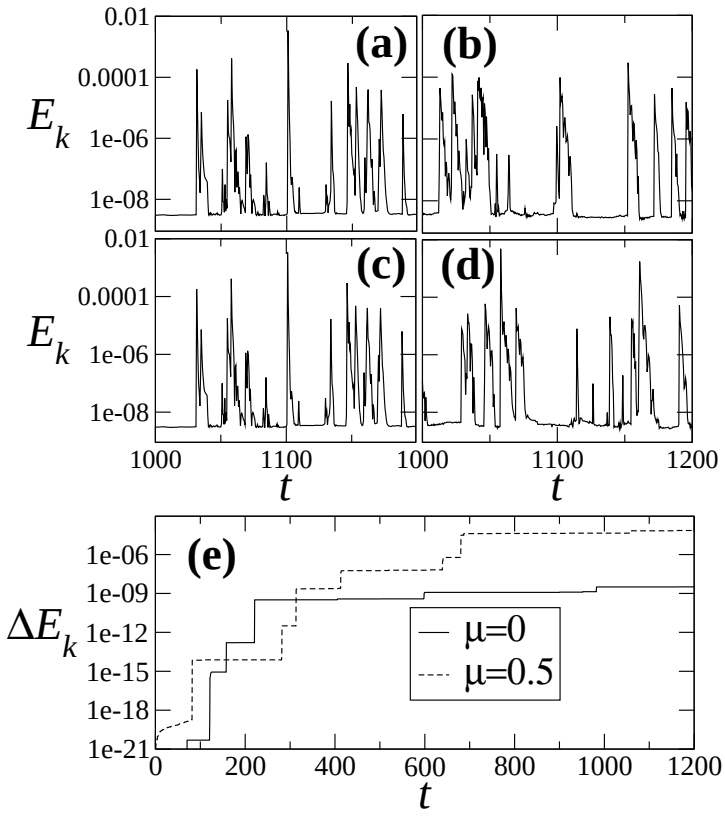

Fig. 3. Dependence of the numerical scheme on the integration step Δt and the friction coefficient μ, by plotting the kinetic energy E_k as a function of time, for **(a)** $\Delta t = 10^{-3}$ s and $\mu = 0$ (no friction), **(b)** $\Delta t = 10^{-3}$ s and $\mu = 0.5$, **(c)** $\Delta t = 5 \times 10^{-3}$ s and $\mu = 0$, and **(d)** $\Delta t = 5 \times 10^{-3}$ s and $\mu = 0.5$. In **(e)** we show the difference between the values of E_k obtained with the two values of Δt. Here, $k_n = 400$ and the parametric relations in Eq. (10) and (11) are used (see text).

The two values of Δt used in Fig. 3 can be written as $\Delta t = 13/500 t_c$ and $13/2500 t_c$. Thus, we conclude that the expected upper limit $\sim t_c/10$ is still too large to guarantee convergence of the integration scheme when friction is considered.

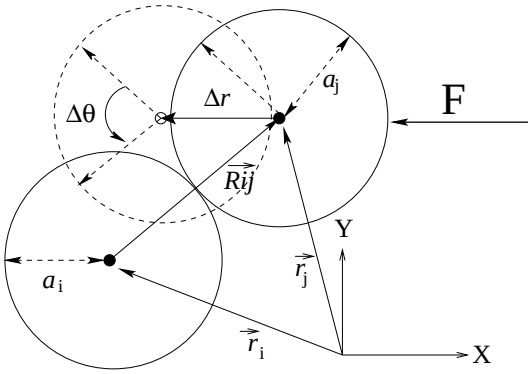

Fig. 4. Sketch of the stress controlled test of two particles (discs). The particle located at $\boldsymbol{r}_i$ remains fixed, while the particle at $\boldsymbol{r}_j$ is initially touching particle i. The vector $\boldsymbol{R}_{ij}$ connecting the center of mass of particles i and j is initially oriented 45^o with respect to the x-axis. After applying the constant force $\boldsymbol{F}$ to disc j, the system relaxes to a new position (dashed circumference). Between its initial and final position particle j undergoes a displacement Δr and a rotation $\Delta\theta$ (see text).

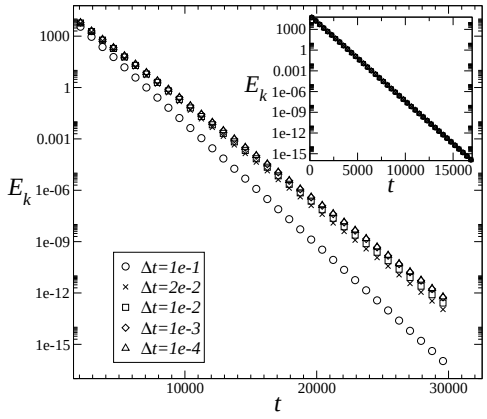

Fig. 5. The relaxation of the system of two discs sketched in Fig. 4. Here we plot the kinetic energy E_k as a function of time t (in units of t_c) for different integration increments Δt and using a stiffness $k_n = 4 \times 10^8$ N/m and a friction coefficient $\mu = 500$. The large μ value is chosen so that the system remains in the elastic regime. As one sees, the relaxation time t_R converges to a constant value when Δt is sufficiently small (see text). This discrepancy between the values of t_R when different integration steps are used does not occur in the absence of friction ($\mu = 0$), as illustrated in the inset. The slope of the straight lines is $-1/t_R$ (see Eq. (13)).

Next we will perform a careful analysis to obtain a proper integration step as function of the parameters of our model. For that, we consider the simple situation of two circular particles and study the kinetic energy of one of them under external forcing, as sketched in Fig. 4. We start with two touching discs, i and j, where one of them, say i, remains fixed, while the other is subject to a force $\boldsymbol{F}$ perpendicular to its surface (no external torque is induced) along the x-axis. As a result of this external force, the disc j undergoes rotation. The contact force is obtained from the corresponding springs that are computed, as described in Sec. 2, and acts against the external force. This results in an oscillation of disc j till relaxation (dashed circle in Fig. 4) with a final center of mass displacement of ΔR and a rotation around the center of mass of $\Delta\theta$. Since $\boldsymbol{F}$ is kept constant, the procedure is stress controlled.

For the two discs sketched in Fig. 4, we plot in Fig. 5 the kinetic energy as a function of time, from the beginning until relaxation, using different integration steps, namely $\Delta t = 10^{-1}, 2\times10^{-1}, 10^{-2}, 10^{-3}$ and 10^{-4} s in units of t_c. As we see, the kinetic energy decays exponentially,

$$E_k(t) = E_k^{(0)} \exp\left(-\tfrac{t}{t_R(\Delta t)}\right), \tag{13}$$

where t_R is a relaxation time whose value clearly depends on the integration step Δt. As illustrated in the inset of Fig. 5, this change in t_R is not observed when friction is absent ($\mu = 0$), since no tangential forces are considered ($F_e^t = 0$).

Next, we will show that this dependence of t_R on Δt vanishes for

$$\Delta t \lesssim T_t(k_n, \mu) t_c, \tag{14}$$

where $T_t(k_n, \mu)$ is a specific function that is determined below. Notice that, in our case, the only free parameters on which T_t may depend are the friction μ and the normal stiffness k_n, since we consider a fixed restitution coefficient in the normal direction, $\epsilon_n = 0.9875$ and fixed relations $k_t/k_n = 1/3$ and $\epsilon_t/\epsilon_n = 1.0053$.

Figure 6a shows the relaxation time t_R of the kinetic energy of the two-particle system for different values of stiffnesses, namely for $k_n = 1, 50, 200, 10^4$ and 10^8 N/m. For all k_n values, one sees that, for decreasing Δt, the relaxation time t_R increases until it converges to a maximum. The stabilization of t_R occurs when Δt is small compared to the natural period $1/\omega_0$ of the system. We define T_t as the largest value of Δt for which we have this maximal relaxation time.

As shown in Fig. 6b, all curves in 6a can be collapsed by using the normalized integration step $\Delta t/t_c$. From Eq. (11) we calculate the contact times corresponding to these k_n values as $t_c = 1.969, 0.278, 0.139, 9.8\times10^{-2}$ and 9.8×10^{-5} s respectively. In fact, as shown in the inset of Fig. 6b the relaxation time scales with the stiffness as $t_c \sim k_n^{-1/2}$ (see Eq. (11)).

From Fig. 6 one can conclude that the relaxation time converges when the integration step obeys Eq. (14) with $T_t = 10^{-3}$ (dashed vertical line in Fig. 6b). We simulate the system also for $\mu = 0.005, 0.005, 0.05, 0.5, 5, 50$ and 500 and similar results were obtained.

In Fig. 6 both translation and rotation of particles are considered. The rotation of particles is usually of crucial interest, for instance to simulate rolling [7, 19].

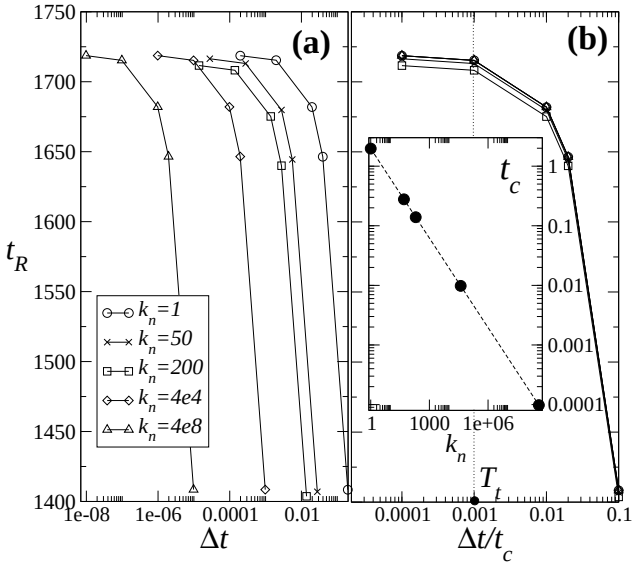

Fig. 6. The relaxation time t_R (in units of t_c) as a function of **(a)** the integration step Δt and **(b)** the normalized integration step $\Delta t/t_c$, where the contact time t_c is defined in Eq. (11). Here the friction coefficient is kept fixed $\mu = 500$ and different stiffnesses k_n (in units of N/m) are considered. The quotient $\Delta t/t_c$ collapses all the curves for different k_n. We find $t_c \sim k_n^{-1/2}$ as illustrated in the inset (see Eq. (11)). As a final result one finds a constant $T_t = 10^{-3}$ (dashed vertical line). For other values of the friction coefficient one observes similar results.

But, suppressing rotation can also be of interest for instance, when simulating fault gouges: by hindering the rotation of particles, one can mimic young faults where a strong interlocking between the constituent rocks is expected [7].

To study this scenario, we present in Fig. 7a the relaxation time for the same parameter values as in Fig. 6, now disabling rotation. Here, we obtain a constant $T_t = 10^{-4}$ also, independent of k_n, one order of magnitude smaller than the previous value in Fig. 6. In other words, when rotation is suppressed, one must consider integration steps typically one order of magnitude smaller than in the case when the discs are able to rotate. This can be explained as follows.

When suppressing rotation, one restricts the system to have a single degree of freedom. All energy stored in the rotational degree of freedom through the integration of the equations of motion is suppressed. This effectively acts like an increase of the friction coefficient, making the system more sensitive to the integration step, i.e. yielding a smaller bound T_t. By comparing Fig. 7a with Fig. 6a, one sees that the relaxation time t_R is smaller when rotation is suppressed.

From the bounds on the integration steps obtained above, one realizes that, in general, the correct integration step must be significantly smaller than usually assumed.

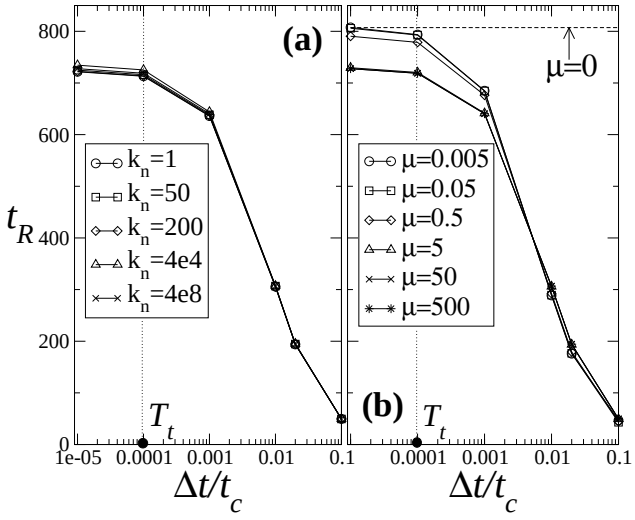

Fig. 7. The relaxation time t_R (in units of t_c) of the kinetic energy as a function of the normalized integration step $\Delta t/t_c$, when rotation is suppressed. **(a)** $\mu = 500$ and different values of k_n and for **(b)** $k_n = 4 \times 10^8$ and different values of μ. The dashed horizontal line $\mu = 0$ in (b) indicates the relaxation time of the kinetic energy in the absence of friction (see text).

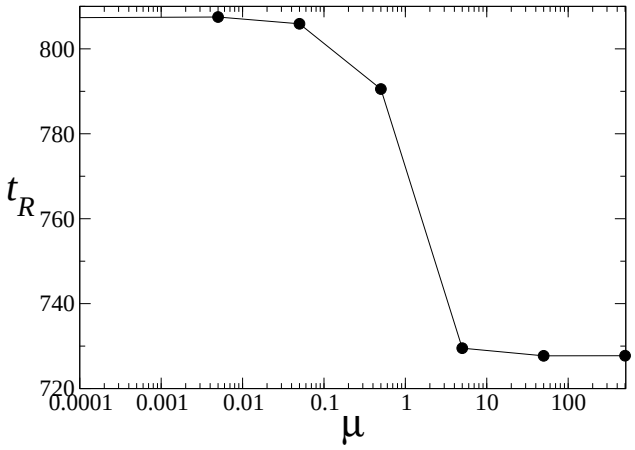

Fig. 8. The relaxation time t_R (in units of t_c) as a function of the friction coefficient μ when rotation is suppressed. Here $k_n = 4 \times 10^8$ N/m which corresponds to a contact time $t_c = 9.8 \times 10^{-5}$ s. The normalized integration step is $\Delta t/t_c = 10^{-5}$.

While Fig. 7a clearly shows that t_R does not depend on the stiffness k_n, from Fig. 7b one sees that the same is not true for the friction coefficient μ. Indeed, from Fig. 8 one sees that there is a change of the relaxation time around $\mu = 1$. Here, the values correspond to a normalized integration step $\Delta t/t_c = 10^{-5}$ for which t_R has already converged. This might be explained by considering the fact that for large values of μ the contact is essentially non-sliding, which induces a faster relaxation than for smaller μ values.

It is important to stress that all the results above were taken within the elastic regime, since the dependence on Δt does not occur when the Coulomb condition is fulfilled (inelastic regime). This fact indicates that the improvements in the algorithm should be implemented when computing the elastic component of the tangential contact force, in Eq. (6), as explained in the next Section.

4 Improved approach to integrate the contact force

In this Section we will describe a technique to overcome the need of very small integration steps. As shown previously, when using Cundall's spring[4], the relaxation time of the two particles only converges when Δt is a small fraction T_t of the contact time t_c. This is due to the fact that the elastic elongation is assumed to be linear in Δt, i.e. the finite difference scheme in Eq. (6) is very low order, $(\Delta t)^2$, compromising the convergence of the numerical scheme that is of order $(\Delta t)^6$. Therefore, the most plausible way to improve our algorithm is by choosing a different expression to compute the elastic tangential elongation ξ without using Eq. (6).

We will introduce an expression for ξ that contains only the quantities computed in the predictor step. In this way we guarantee that ξ has errors of the order of $(\Delta t)^6$, instead of $(\Delta t)^2$, as it is the case of Eq. (6). Let us illustrate our approach on the simple system of two discs considered in the previous Section (see Fig. 4).

On one side, if rotation is not allowed, the elastic elongation ξ depends only on the relative position of the two particles. In this case we substitute Eq. (6) by the expression

$$\xi_j^{(tr)}(t+\Delta t) = \xi_j^{(tr)}(t) + \frac{a_i}{a_i + a_j}(\boldsymbol{R}_{ij}^p(t+\Delta t) - \boldsymbol{R}_{ij}^p(t)) \cdot \hat{t}^c, \qquad (15)$$

where a_i and a_j are the radii of the discs i and j respectively, $\boldsymbol{R}_{ij}$ is the vector joining both centers of mass and points in the direction $i \to j$ (see Fig. 4). Index p indicates quantities derived from the coordinates computed at the predictor step.

On the other side, if $\boldsymbol{R}_{ij}$ is kept constant and only rotation is possible, particle j will have an elongation ξ that depends only on its rotation between time t and the predictor step:

$$\xi_j^{(rot)}(t+\Delta t) = \xi_j^{(rot)}(t) + (\theta_j^p(t+\Delta t) - \theta_j^p(t))a_j, \qquad (16)$$

where θ^p and $\theta(t)$ are the angles of some reference point on particle j at the predictor step and at time t respectively.

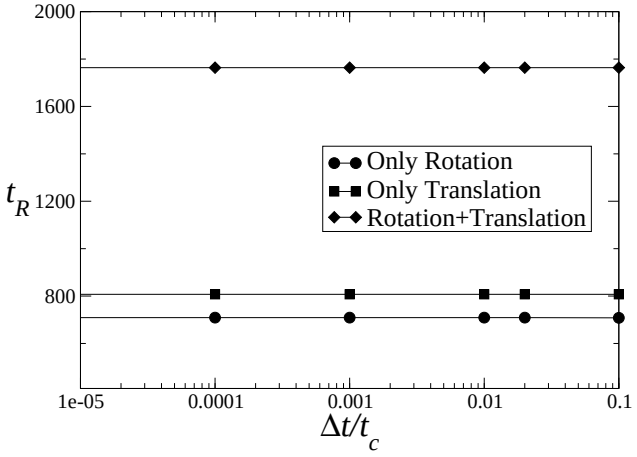

Fig. 9. The relaxation time t_R (in units of t_c) using Eqs. (15) and (16) between two discs, as illustrated in Fig. 4. For the three cases when considering only rotation, only translation or both, the relaxation time remains constant independent of the integration step.

When both translation and rotation of particle j occur, then the elongation is the superposition of both contributions, yielding $\xi_j = \xi_j^{(tr)} + \xi_j^{(rot)}$.

Figure 9 shows the relaxation time t_R as a function of the integration step for the three situations above, namely when only rotation is considered, when only translation is considered and when both rotation and translation are allowed. As we see for all these cases, the relaxation time is independent on the integration step. This is due to the fact that all quantities in the expression for ξ above are computed at the predictor step which has an error of the order of $(\Delta t)^6$, i.e. the error $(\Delta t)^2$ introduced in Eq. (6) is now eliminated. Therefore, with the expressions in Eqs. (15) and (16) one can use integration steps significantly larger than with the original Cundall spring.

When considering discs, one does not take into account the shape of the particles. Next, we consider the more realistic situation of irregular polygonal-shaped particles. Motion of rigid particles with polygonal shape is more complicated than that of simple discs, since the contact point no longer lies on the vector connecting the centers of mass. Further, for polygons, one must also be careful when decomposing the dynamics of each particle into translation and rotation around its center of mass. This implies recalculating each time the position of the center of mass (only from translation) and the relative position of the vertices (only from rotation).

Therefore, for the translational contribution $\xi^{(tr)}$ in Eqs. (15), we compute the overlap area between the two particles at t and at the predictor step. The overlap area is in general a polygon with a geometrical center that can be computed also at time t and the subsequent predictor step, yielding $\boldsymbol{r}_c(t)$ and $\boldsymbol{r}_c^p$ respectively. The increment for the translational contribution will be just the tangential projection $(\boldsymbol{r}_c(t) - \boldsymbol{r}_c^p) \cdot \hat{t}^c$. Similarly, the contribution from the (polygonal) particle rotation is computed by

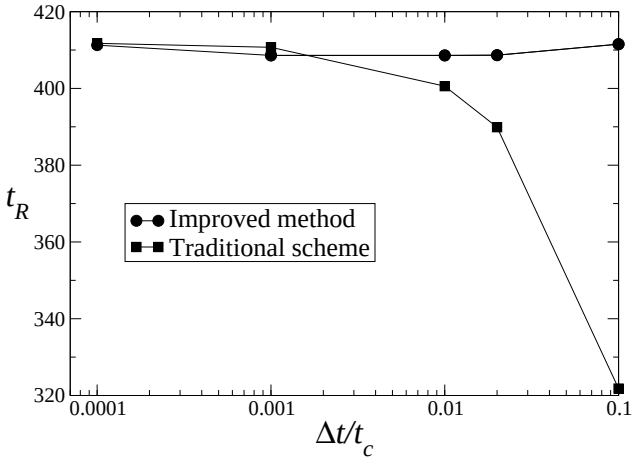

Fig. 10. Stress control test between two polygonal particles, as illustrated in Fig. 1. Comparison of the relaxation time t_R (in units of t_c) when using the standard integration scheme (squares) and the proposed improved scheme (circles). Here, rotation is neglected.

determining branch vectors, $\boldsymbol{r}_b(t)$ and $\boldsymbol{r}_b^p$, defined as the vectors joining the center of the particle and the center of the overlap area at time step t and the predictor step respectively. Computing the branch vector at t and at the predictor step, one derives the angle defined by them, namely $\theta = \arccos\left(\boldsymbol{r}_b^p \cdot \boldsymbol{r}_b(t)/(r_b^p r_b(t))\right)$ and the average value $(r_b^p - r_b(t))/2$, yielding an increment in Eq. (16) given by $\theta(r_b^p - r_b(t))/2$.

Figure 10 compares how the relaxation time varies with the normalized time step when the original Cundall approach is used (squares) and when our improved approach is introduced (circles). Clearly, the dependence on the integration step observed for the usual integration scheme disappears when our improved approach is introduced. Therefore, all the conclusions taken above for discs remain valid for polygons.

5 Discussion and conclusions

In this paper we introduced a technique to improve the accuracy of the numerical scheme used to compute the evolution of particle systems.

To that end, we have first shown that the range of admissible integration steps has an upper limit significantly smaller than typically used. The accuracy of the numerical scheme not only depends on the associated error when computing the particle positions (predictor-corrector scheme), but also on the accuracy when determining the frictional force, which is usually implemented by the Cundall spring. Since the Cundall spring is linear in the integration step, the overall accuracy of the numerical

scheme cannot be higher than $(\Delta t)^2$. Therefore, when large integration steps are required, e.g. in slow shearing, the numerical scheme does not give accurate results.

To overcome this problem we introduced an alternative approach for computing the frictional forces that suits not only the simple situation of discs but the more realistic situation of polygonal particles. Our approach is particularly suited for situations where non-sliding contacts are relevant to the overall response. In general, for any other integration scheme, the substitution of the Cundall spring expression by the relations introduced in Eqs. (15) and (16), yields an error that is of the same order of the one associated with the predictor-corrector scheme.

Inspired by the above results, some questions arise to further improve our approach. First, the influence of the relations k_t/k_n and ϵ_t/ϵ_n should also be considered. Preliminary simulations have shown that the upper limit for the integration step increases with the value of k_t/k_n. Second, the test assumes a unique choice for the position of the contact point. However, in a system under shearing the integration must be also performed before the appearance of new contacts. The initial contact point of a new contact will depend on the size of the integration step. This point should also be taken into account within our new approach, either by assuming some sort of interpolation or by using an event-driven scheme till the first contact point. Third, there is the problem of how to better define the contact point between two polygons. Since the contact point is taken as the geometrical center of their overlap area, the branch vectors also vary during rotation, which is not taken into account in our present approach. These and other points will be addressed in the future.

Acknowledgments

The authors thank Fernando Alonso-Marroquín for useful discussions. We thank support by German-Israeli Foundation and by *Deutsche Forschungsgemeinschaft*, under the project HE 2732781. PGL thanks support by *Deutsche Forschungsgemeinschaft*, under the project LI 1599/1-1. HJH thanks the Max Planck prize.

References

1. T. Pöschel and T. Schwager, *Computational Granular Dynamics* (Springer, Berlin, 2005).
2. M.P. Ciamarra, A. Coniglio, M. Nicodemi, Phys. Rev. Lett. **94** 188001 (2005).
3. F. da Cruz, S. Eman, M. Prochnow, J.N. Roux Phys. Rev. E. **72** 021309 (2005).
4. P.A. Cundall, Ingenieur-Archiv **59**, 148 (1989).
5. P.A. Thompson, G.S. Grest, Phys. Rev. Lett. **67** 1751 (1991).
6. A.A. Peña, R. García-Rojo, H.J. Herrmann, Granular Matter, **9**:279-291 (2007).
7. F. Alonso-Marroquín, I. Vardoulakis, H.J. Herrmann, D. Weatherley, P. Mora, Phys. Rev. E **74**, 031306 (2006).
8. P. Mora, D. Place, Geophys. Res. Lett. **26**, 123 (1999).
9. S. McNamara, R. Garía-Rojo and H.J. Herrmann, submitted to Phys. Rev. E, 2007.

10. M.P. Allen and D.J. Tildesley, *Computer Simulation of Liquids* (Oxford Univ. Press, Oxford, 2003).
11. S. Luding, E. Clément, A. Blumen, J. Rajchenbach, J. Duran, Phys. Rev. E **50**, 4113 (1994).
12. P.A. Cundall and O.D.L. Strack, Géotechnique **29**, 47-65 (1979).
13. E. Rougier, A. Munjiza, N.W.M. John, Int. J. Numer. Meth. Eng. **61**, 856 (2004).
14. S.F. Foerster, M.Y. Louge, H. Chang, K. Allia, Phys. Fluids **6(3)**, 1108 (1994).
15. S. Luding, in *Physics of Dry Granular Media*, H.J. Herrmann, J.-P. Hovi, and S. Luding (Kluwer Academic Publishers, Dordrecht, 1998), pp. 285.
16. H.-G. Matuttis, Granular Matter **1**, 83 (1998).
17. H.J. Tillemans, H.J Herrmann, Physica A **217**, :261-288 (1995).
18. F. Alonso-Marroquín and H.J. Herrmann, Phys. Rev. Lett. **92**, 054301 (2004).
19. S. Latham, S. Abe, P. Mora, in R. García-Rojo, H.J. Herrmann, and S. McNamara (eds.), *Powders and Grains 2005*, (Balkema, Stuttgart, 2005) pp. 213.